2011

Measurements and Prediction of Thermal Contact Resistance across Coated Joints

C. Merrill

S V. Garimella
Purdue University, sureshg@purdue.edu

Follow this and additional works at: http://docs.lib.purdue.edu/coolingpubs

Measurement and Prediction of Thermal Contact Resistance Across Coated Joints[*]

Christine T. Merrill and Suresh V. Garimella[†]

Cooling Technologies Research Center, School of Mechanical Engineering

Purdue University, West Lafayette, Indiana 47907 USA

ABSTRACT

An integrated experimental and numerical investigation of the thermal contact resistance across two nominally flat, coated metallic engineering surfaces in contact is presented. The model consists of a surface deformation computation which determines the actual contact area and number of contacting asperities at a joint, and a constriction resistance analysis which determines the constriction resistance through each individual contacting asperity. Predictions from the model are validated against experiments conducted for the purpose. The experiments are performed according to a Design of Experiments approach, and evaluated using statistical regression. Three substrates (copper, brass, and aluminum) and three coatings (silver, nickel and tin) are considered with a variety of coating thicknesses and substrate roughnesses. The contact load is also varied. The experimental measurements show that the best choice of a coating for contact resistance mitigation depends on the substrate material and roughness, and cannot be prescribed in general. A regression equation developed for the experimental results offers a useful tool for the design of coated contacts. The measured results agree well with predicted values from the numerical model, especially in cases of a rough substrate or hard coating.

INTRODUCTION

Due to the microscopically rough nature of any engineering surface, the actual contact area between two conforming surfaces is a small fraction of the nominal contact area, usually only 1-2% [1]. Generally, a gas such as air fills the interstitial area where the surfaces are not in contact. In some applications, the gaps may be in vacuum. Heat transfer can occur by four modes across such contacts: conduction through the contact spots, conduction and convection through the gas gap between the surfaces, and radiation between the surfaces. The gas gap is usually only a few micrometers in thickness, so that convection may be neglected [2]. While radiation and conduction through the gas gap can contribute to heat transfer across the contact, conduction through the solid spot contacts is the dominant heat transfer mode, and much of the heat flow is constrained to flow through these spots. The presence of an interstitial gas can mitigate this constriction to some extent.

The study of contact resistance is of interest in varied applications [3,4,5]. In the thermal management of electronics, the effectiveness of heat removal from the electronic components to heat spreaders, heat sinks, or other heat removal and spreading devices is adversely affected by contact resistance. Nuclear reactors encounter contact resistance between the fuel elements and their cans. In these and many other applications, the mitigation of contact resistance is highly desired.

Thermal contact resistance is defined as the ratio of the temperature drop across a joint between two surfaces in contact to the heat flux through the joint. The increased temperature difference across a joint relative to that which would be seen if the contact were perfect is known as the temperature jump, ΔT_{jump}. Thus,

$$R''_{contact} = \frac{\Delta T_{jump}}{Q''} \qquad (1)$$

Several factors are known to influence the contact resistance at a joint. The surface topography of the two mating surfaces, which determines the number and size of contact spots, is a primary factor. Macroscopic waviness, if present, can greatly decrease the amount of contact. Thermal and mechanical properties such as thermal conductivity, elastic modulus and surface microhardness play an important role. Contact resistance is strongly influenced by the contact pressure, and is weakly influenced by the interface temperature [6]. Generally, the contact resistance decreases with temperature [4]. Parmenter and Marschall [6] performed experiments

2

on bare aluminum and stainless steel surfaces. They investigated microhardness, roughness, contact pressure and surface contamination effects on thermal contact resistance. Singhal et al. [5] considered a broader range of parameters and materials, but the contact continued to be between bare metallic surfaces. The present study builds on the work of Singhal et al. by investigating the effect of a soft metallic coating at the joints.

Because thermal contact resistance is unacceptably high with bare-surface contact in many applications, several strategies for the reduction of this resistance have been adopted. The most common approach is to introduce an interface material to improve heat transfer. Interface materials fall into three broad categories: metallic coatings, thermal pads or foils, and thermal greases or pastes. All such materials reduce contact resistance by replacing the interstitial gas with a material of higher thermal conductivity, thus decreasing constriction of the heat flow lines through the contact spots. Thermal greases and pastes suffer from the drawback that they tend to migrate from an interface over time. Pads and foils must be installed carefully to avoid unintended increases in contact resistance due to misplacement. Metallic coatings may be preferable in many applications because of their permanent nature and potential ease of standardized application. A metallic coating applied to a surface for the purpose of contact resistance mitigation is generally a soft metal of high thermal conductivity. The softness allows deformation upon the application of pressure such that the gas gap is displaced by the more thermally conductive metal.

The effects of metallic coatings on contact resistance have been experimentally explored in the literature. Antonetti and Yovanovich [7] performed experiments with a silver coating on nickel substrates over a range of roughnesses and coating thicknesses. Their work involved a coating only on one of the surfaces in contact, at low contact loads. Kang et al. [8] performed experiments involving aluminum substrates, with lead, indium and tin coatings. Chung [9] and Chung and Sheffield [10] investigated a larger variety of coatings on aluminum substrates: aluminum, lead, indium, copper, silver, and copper and silver phase change materials. These experiments included coatings on one and two sides, and were performed at very low contact loads. Li et al. [11] considered a wider range of substrates with experiments on stainless steel and machine steel specimens coated with tin, copper, silver and aluminum. Experiments have also been reported on anodized aluminum samples, such as those of Peterson and Fletcher [12] at high loads and Lambert et al. [13] at low loads. A number of conclusions have been drawn

based on these experimental studies. Rough surfaces, as expected, exhibited greater contact resistances than smoother ones. The microhardness of the substrate and coating were shown to be important material properties, as were the thermal conductivities of the coating and substrate.

Because a comparative analysis of past experimental studies is difficult due to the difference in substrates, coatings, surface roughnesses, thicknesses and contact loads considered in each study, one aim of the present work is to provide a broader understanding of these parameters as they relate to each other on a common platform of tests.

Antonetti and Yovanovich [7] presented the first comprehensive thermomechanical model for coated-surface contact resistance. This model consisted of two primary parts: an analytical solution to the constriction resistance through a single asperity, and a plastic deformation model to compute the size of the average asperity on a surface of given roughness and asperity slope and the number of asperities in contact. The surface deformation model assumes that the coated surface can be reduced to an equivalent bare surface by computing an effective microhardness for the substrate/coating combination. Microhardness varies with depth of indentation: initially, it is essentially the hardness of the coating material, but gradually changes as the effect of the substrate comes into play. At a large indentation depth, the effective microhardness is that of the substrate. The effective microhardness is determined by using hardness measurements at varying depths from a similar specimen. An equation can then be written to relate effective hardness to indentation depth. Because the indentation depth is dependent on the hardness of the material and determines the size of a contact spot, the indentation depth and effective microhardness must be solved for iteratively.

The surface deformation model developed by Antonetti and Yovanovich calculates the average contact spot size based on the assumption of a Gaussian asperity distribution. This assumption is quite adequate when no knowledge of the actual surfaces is available. However, many tools are readily available today that allow detailed surface characterization. For example, bead blasting, grinding, milling and turning will all produce very different surface profiles. A profile scan can provide the height and shape of the individual asperities. Thus, a model taking advantage of this more detailed surface information could lead to more accurate predictions, and also provide greater insight into the mechanisms contributing to contact resistance. Moreover, the surface deformation model of Antonetti and Yovanovich assumes only plastic deformation in

4

the coating and substrate, which may not hold if the substrate is hard and the contact load is small.

The present work is an integrated experimental and numerical investigation of thermal contact resistance across metallically coated joints. A Design of Experiments approach is employed to obtain an understanding of the parameters governing contact resistance and their interactions with each other. In conjunction, a thermomechanical model is developed which uses scans of rough surfaces to estimate the actual contact area at the joint and predict the thermal contact resistance based on elastic and plastic deformation models. The contributions of this work are a large experimental database, a correlation equation based on the experimental results, and an experimentally validated predictive model for the thermal contact resistance across coated joints.

EXPERIMENTAL INVESTIGATION

The experiments were designed to cover a wide range of parameters so that a comprehensive database may be generated. A Design of Experiments (DOE) approach was used to minimize the number of experiments needed while yielding the best understanding of the factors involved in coated-joint contact resistance. Five parameters were studied: surface roughness, coating thickness, coating material, substrate material and contact load.

Design of Experiments

Because of the large number of independent parameters to be studied, a full-factorial experimental program would be prohibitively time-consuming. A DOE-based test matrix was chosen to reduce the number of experiments needed. A D-optimal design using the coordinates exchange algorithm in MATLAB with 4 variables (contact load was excluded from the experimental design) was used to generate a test matrix, which is shown in Table 1. Brass, aluminum and copper were selected as substrate materials. Coating materials were chosen, based on industry recommendations, as nickel, tin, and silver. Surfaces ranged in roughness from 1 to 15 μm Ra. Coating thicknesses were selected to be 1, 3, and 5 μm, based again on recommendations from industry. With this design, a total of 15 sample pairs were required, as shown in Table 1. These samples were tested over a range of loads from approximately 0.5 MPa to 5 MPa.

Experimental Setup

Li et al. [11] introduced a Figure of Merit for ranking materials used in contact-resistance mitigation applications. They suggested that the ratio of thermal conductivity to microhardness, k/H, accurately reflected the effect of each property. Microhardness is reported as a Vickers hardness number (VHN), with units of kgf/mm^2. As thermal conductivity increases, constriction resistance is mitigated, and likewise, as microhardness decreases, the total contact area increases which results in less constriction resistance. Table 2 shows numerical values for this Figure of Merit for the materials considered here.

The test samples were manufactured in a manner similar to that described by Singhal et al. [5] for uncoated surfaces. Surface roughness was measured using a Surfanalyzer 5400 surface profile scanner. Next, the samples were electroplated with the desired coating materials by Honeywell, Inc. For the aluminum substrate, adhesion was improved using a flash layer of nickel below the silver or tin coatings. To minimize oxidation of the coatings before testing, the samples were stored in an inert mineral oil which prevented oxygen from reaching any surface of the test samples. Each sample was carefully cleaned of oil before testing. One of the samples (Sample #8) was removed from the DOE analysis due to possible contamination of the coating that led to inconsistent results. The contact resistance measurements were obtained using the test apparatus described in Singhal et al. [5]. This apparatus, shown schematically in

Figure 1, induces axial heat flow through two test samples and two heat-flux meters by means of a heater at one end of the test column and a chiller at the other end. A load cell measures the contact load and a radiation shield reduces losses from the column. The heat flux through the column is measured by two cylinders of electrolytic iron (National Institute of Standards and Technology Research Material 8420/8421), a material for which the thermal conductivity is well known as a function of temperature. These cylinders are instrumented with thermocouples to measure the temperature gradient. This temperature gradient is used along with the known thermal conductivity of electrolytic iron to compute the heat flux through the column. The temperature gradient is likewise measured through the test samples, and the temperature at the interface obtained by extrapolation using a least-squares fit. Other details of the experimental apparatus and procedures are available in Singhal et al. [5].

The temperatures at the interface may be obtained from extrapolations conducted in several alternative ways, two of which are shown in Figure 2. If the temperatures are extrapolated from the test sample thermocouple locations without regard to the presence of the coating, then the temperature jump ΔT_1 would result. The other temperature jump ΔT_2 shown in the figure is the correct value, since it reflects the different thermal conductivities of the coatings (from each other and from the substrate), as well as the small resistances at the substrate/coating interfaces. It is emphasized that these effects are exaggerated in the illustration. Cecco and Yovanovich [14] showed that the actual thermal resistance of a "perfect" joint is two orders of magnitude less than typical constriction resistance values encountered between rough surfaces. Thus, contact resistance between the substrate and coating can be neglected. Also, the temperature difference across the coatings is negligible for the coating thicknesses considered here. For example, the temperature difference across a 5μm thick tin coating is merely 0.27% of the total temperature difference for a typical experimental condition. Therefore, ΔT_1 is used as an excellent approximation of ΔT_2 in this work.

The criterion used to determine when a steady-state temperature distribution has been reached, as well as the data acquisition methods, are described in detail in Singhal et al. [5]. Results were obtained at 222 N loading intervals over the range of 222 N – 2669 N. A number of repeated tests were run on several of the samples to ensure repeatability of results. The thermal contact resistance at the interface was computed as

$$ R = \frac{T_{1,average} - T_{2,average}}{(Q_{FM1} + Q_{FM2})/2} \tag{2} $$

The temperatures $T_{1,average}$ and $T_{2,average}$ correspond to the extrapolated temperatures on either side of the contact, and Q_{FM1} and Q_{FM2} represent the heat flow rate through each flux meter.

Uncertainty Analysis

A detailed uncertainty analysis was carried out as explained in Singhal et al. [5]. The uncertainty in the contact resistance measurement is given by

$$ U_{R_{contact}} = \left[\left(\frac{U_{T_d}^2}{\left(T_d - T_e\right)^2} + \frac{U_{T_e}^2}{\left(T_d - T_e\right)^2} + \frac{U_{Q_{avg}}^2}{Q_{avg}^2} \right) \times R_{contact}^2 \right]^{1/2} \tag{3} $$

where T_d and T_e represent the extrapolated temperatures on either side of the joint. The average heat flow rate through the column is represented by Q_{avg}. The uncertainty in the extrapolated temperatures is shown to be dependent on the uncertainties in thermocouple reading and in thermocouple location. Likewise, the uncertainty in heat flux is a function of the uncertainties in the extrapolated surface temperatures in the flux meters, the flux meter diameter, and its thermal conductivity. The average uncertainty, $U_{Rcontact}/R_{contact}$, is 0.279, with maximum and minimum values of 1.474 and 0.027, respectively, and a median value of 0.121.

Experimental Results

The impact of the coatings on contact resistance is examined by comparing the coated-joint results to those of a corresponding 1 μm Ra bare sample, as measured by Singhal et al. [5]. In Figure 3, results of all the experiments with aluminum substrates are shown. In all cases, a coated sample with 1 μm roughness has a lower contact resistance than the bare sample. The degree of improvement depends on the coating thickness and material. Rougher coated samples do not exceed the performance of the 1 μm rough bare sample. However, the 5 μm rough sample coated with 1 μm of silver has nearly identical contact resistance as the 1 μm rough bare sample. The 15 μm rough surfaces coated with aluminum also improve in performance to nearly the same extent as a 1 μm rough uncoated surface. Nickel, though a common plating material, has the least impact on contact resistance, while both silver and tin have a much larger positive effect.

Figure 4 shows the results of tests on the copper substrates. Again, the results are compared to a 1 μm rough bare copper sample. In this case, tin is the coating which has the greatest beneficial effect on contact resistance. Silver has mixed results, perhaps because of the effect of other parameters in the selected tests such as the coating thickness (dictated by the DOE test matrix). Nickel again shows the least benefit. These conclusions will be explored more quantitatively in the DOE analysis that follows.

An important observation from the experiments is that the quality of coating is critical to the improvement of contact resistance, as illustrated in Figure 5. After initial plating, some samples were observed to have a poor quality of coating. These samples were stripped and re-coated. Test results from before and after re-plating show the importance of coating quality. With a poor coating, contact resistance values can increase by as much as an order of magnitude. The reason for this is likely the porosity present in a poor coating. This leads to air voids in the coating,

allows the substrate to oxidize, increases the chances of chemical reaction between the coating and substrate, and reduces interface contact area.

The experimental results were evaluated using a commercial software package for DOE analysis, DOE KISS 97 [15]. The analysis was performed using 70 data points from 14 sample pairs over a variety of loads. Five independent variables were correlated: Load, roughness, coating thickness, H/k_s and H/k_c. The dependent variable was contact resistance, R.

The quality of the resulting regression equation is illustrated in Figure 6. The predicted values for contact resistance generally lie close to the experimental values, showing the regression equation to be a good statistical fit, with a correlation coefficient R^2 of 0.91; when adjusted for a small sample size, $R^2 = 0.89$. The standard error of the equation is 0.0045 K/W. The significance of each of the five parameters in the equation was investigated statistically, as was the effect of parameter interactions. This analysis showed that all five parameters (load, coating material, coating thickness, substrate material and substrate roughness) were significant factors in the contact resistance. Some parameter interactions were also significant, and will be discussed below. Two-way interactions investigate the way two parameters affect each other, whereas quadratic effects consider non-linear tendencies of a single parameter. By taking into account all two-way interactions but neglecting three-way and quadratic effects (due to their statistical insignificance), the regression equation becomes

$$
R = \left(
\begin{aligned}
&0.3929 - 0.0592\frac{H_{coat}(VHN)}{k_{coat}(W/mk)} - 0.0590\frac{H_{subs}(VHN)}{k_{subs}(W/mk)} - 0.022Ra(\mu m) + \\
&0.0782t(\mu m) - 0.0844L(MPa) + 0.0068\frac{H_{coat}(VHN)}{k_{coat}(W/mk)}Ra(\mu m) + \\
&0.0623\frac{H_{subs}(VHN)}{k_{subs}(W/mk)}Ra(\mu m) + 0.0066\frac{H_{coat}(VHN)}{k_{coat}(W/mk)}t(\mu m) - \\
&0.0941\frac{H_{subs}(VHN)}{k_{subs}(W/mk)}t(\mu m) - 0.028\frac{H_{subs}(VHN)}{k_{subs}(W/mk)}L(MPa) + \\
&0.0097L^2(MPa^2) - 0.0036Ra(\mu m)t(\mu m) + \\
&0.0010Ra(\mu m)L(MPa) + 0.0757\frac{H_{coat}(VHN)}{k_{coat}(W/mk)}\frac{H_{subs}(VHN)}{k_{subs}(W/mk)}
\end{aligned}
\right)^2
\tag{4}
$$

where the units on the input values are as specified. Because this equation is simply a regression fit of experimental data, and is not derived based on physics, the equation must be used with the units with which it was generated.

Along with the development of this regression equation, the effect of each parameter on the experimental results can also be explored in the DOE analysis. Some parameters were found to have strong interactions, meaning that the effect of one parameter strongly influenced that of another. Such parameter-interaction studies show a strong connection between the effect of surface roughness and coating thickness on contact resistance. At a low surface roughness, a thin coating produces a smaller contact resistance than a thick coating. However, as the surface roughness increases, a thicker coating has a lower resistance than a thin coating. This is likely because a thicker coating deforms more to fill the larger gaps of the rough surface, whereas a thin coating lacks sufficient material to fill these gaps. With a smoother surface, the extra coating thickness is not necessary. Likewise, there is a significant interaction between substrate material properties (H/k_{sub}) and coating thickness. When H/k_{sub} is small (a desirable substrate) a thin coating performs better; however, as the substrate quality decreases, the thicker coating becomes more effective. These interactions help provide a better understanding of the contact resistance across coated joints.

THERMOMECHANICAL MODELING

The methodology for predicting contact resistance of coated joints follows the approach developed by Singhal et al. [5] for bare surfaces, and is summarized as follows:

1. Using surface scan data, a 3-dimensional surface is created.
2. The number and heights of asperities on the surface are calculated.
3. A surface deformation model computes the size and number of contacting asperities.
4. A constriction resistance model computes the constriction resistance for each of the contacting asperities.
5. The total contact resistance is found by summing all the constriction resistances in parallel.

The method of constructing a 3-dimensional surface from surface scan data, as well as that of determining the number and heights of individual asperities, is discussed in detail in Singhal et al. [5], and is not repeated here. Steps 1 and 2 are the same regardless of whether the surface is metallically coated or bare.

The determination of total contact area of a joint requires a knowledge of the material properties and topography of the contacting surfaces. Hence, measurement of the surface

topography and microhardness is an important pre-requisite to surface deformation modeling. The hardness of a material varies greatly with depth from the surface, and the surface hardness, or microhardness, is usually many times greater than the bulk hardness [16]. This effect has been attributed to factors such as work hardening and oxidation of the surface. Since asperity deformation takes place in the first few μm of material near the surface, microhardness values should be used instead of bulk hardness values in this prediction.

Microhardness is not a unique material property and must be measured for each surface of interest. Surface microhardness measurements were obtained on four samples prepared especially for surface hardness measurements. These tests were conducted using a M-400-H Vickers Hardness testing machine. The samples were manufactured in an identical fashion to the samples used in the experimental program, except that the substrate was polished instead of bead-blasted since microhardness testing requires a very smooth surface. Nickel, silver and tin coatings were deposited on the polished aluminum substrates, and an additional sample of silver on a copper substrate was fabricated to examine the effect of the substrate on the hardness curve. Tests were conducted over a range of loads, from 10 grams to 500 grams, to generate a hardness curve over a range of indentation depths, as described by Antonetti and Yovanovich [7]. Microhardness values from these tests are summarized in Table 3, along with the corresponding bulk hardness values from [17]. As the hardness of a surface varies with depth of indentation, it is difficult to determine the value for hardness that should be used for a material. Yovanovich et al. [16] introduced the idea of an effective hardness, which is the hardness seen by an indenter at a specific indentation depth on a given surface. Instead of using a single hardness value for a surface, it was suggested that the variation of hardness with depth must be taken into account. Chang [18] further explained the need for using an effective surface hardness, as being a way to account for the increase in the hardness of a thin-film coating due to the strength of the substrate. Because the substrate is generally harder than the coating, the substrate has a strengthening effect on the coating. This is also observed empirically since the effective hardness of a soft coating increases with indentation depth.

Table 4 lists curve-fit equations for hardness from four substrate/coating combinations: Silver on aluminum, nickel on aluminum, tin on aluminum and silver on copper. Figure 7 shows the hardness curves for these coating-substrate pairs. The abscissa is t/d, the relative coating thickness. Several conclusions can be drawn from these curves. Because silver is softer than

11

aluminum, the effective microhardness decreases as the relative coating thickness increases. It can therefore be inferred that a thicker coating can lead to better heat transfer until the bulk thermal resistance of the coating becomes larger any contact resistance mitigation that is realized. A tin coating on an aluminum substrate exhibits a similar behavior of decreasing microhardness with increasing thickness. In this case, the drop-off is more marked because of the large difference between the microhardnesses of the two materials. A different trend is observed for a hard nickel coating on a softer aluminum substrate. In this case, a thin coating would likely be better for decreased resistance. Figure 7 also shows the curve for a silver coating on a copper substrate. This curve has a very different shape than the one seen for silver on an aluminum substrate. This illustrates why hardness curves are needed for specific material pairs, instead of a single equation to be used for all coating/substrate combinations. In these graphs, the measured microhardness is shown as plotted data points. The bulk hardness values are also shown for nickel, silver, aluminum and tin, to illustrate the way that the microhardness varies between the hardness of the coating and that of the substrate as the depth of indentation increases.

The results of these tests show that microhardness values for coated surfaces differ greatly from reported bulk values. This highlights the importance of obtaining actual hardness measurements for use in predictive models. The hardness of a surface governs how much actual contact area is present at a joint because a softer surface will deform more under a given load than a harder surface. These tests also show the strengthening effect due to a hard substrate on a soft coating.

The present work uses a three-dimensional surface created from the surface profiles in the predictions, rather than merely single values for the measured surface roughness and asperity slope. The surface profile measurements were obtained using a Surfanalyzer 5400, a stylus-based two-dimensional profilometer. Information obtained from these surface scans includes the RMS surface roughness, average asperity slope, and a surface profile; only the surface profile is used as an input to the predictive model. Three scans each in orthogonal directions are used to generate a three-dimensional surface as described in Singhal et al. [5].

Scans were obtained for all the samples used in the tests. Scans taken before coating, after coating but before testing, and after testing had similar profiles, roughnesses and asperity slopes. Thus, a thin coating does not affect the surface profile.

12

The surface deformation model in this work is based on the theory developed by Chang [18] for elastic-plastic contact of a rough surface with an ion-plated soft metallic coating.

Figure 8 (a) illustrates the schematic contact of asperities with a flat coated surface. Although the actual contact in the experiments involves two rough surfaces, Singhal et al. [5] showed that two rough surfaces in contact can be reduced to a flat surface and an equivalent rough surface. Chang argued that the particular side of the joint which carries the coating is immaterial in generating an equivalent contact. Chang's model assumes that because the coating is generally relatively soft, it will deform plastically under even the lightest of loads. **This assumption holds even for harder coatings if the coating is thin and the loads are significant (such as in the ranges considered here).** As the asperity penetrates to the substrate, the coating material will be piled up outside the contact region. Thus, as the asperity touches the substrate, the deformation is expected to be initially Hertzian. This was shown to be true through finite element analysis by Tian and Saka [19]. When the asperity penetration is such that the elastic limit of the substrate material is exceeded, the deformation will become elastic-plastic. The main difficulty, then, is the determination of the contact area between an asperity and the coated surface as a function of indentation depth. With a known contact area, the contact load can be determined.

There are two possible modes of substrate deformation. Initially, deformation is elastic, but becomes elastic-plastic as the indentation deepens. It is necessary to determine what mode of deformation is occurring at a given indentation depth. When the depth of indentation, δ, is less than or equal to the coating thickness, t (or, the indenter does not penetrate through to the substrate), the deformation is plastic. When δ is greater than t, but still less than the elastic limit of the substrate, the deformation is elastic. The depth of indentation at the beginning of elastic-plastic deformation in the substrate is found from Hertzian theory [20] as

$$\delta_c = \left(\frac{\pi K Y}{2E'}\right)^2 R \qquad (5)$$

The yield coefficient, K, is a function of Poisson's ratio, and can be linearly approximated as

$$K = 1.2821 + 1.158\nu \qquad (6)$$

It is necessary to use an effective Young's modulus, which is found by

$$\frac{1}{E'} = \frac{1-v_1^2}{E_1} + \frac{1-v_2^2}{E_2} \tag{7}$$

where E_1 and E_2 are the Young's moduli of the two contact surfaces.

When δ is less than or equal to δ_c (from Eq (5)) the deformation is elastic. When δ is greater than δ_c, the deformation is elastic-plastic.

For the plastic deformation in the coating, the contact area and the contact load for an asperity [20] are given by:

$$A = 2\pi R\delta \tag{8}$$

$$P = H_c A \tag{9}$$

Deformation in the substrate is complicated by the added coating layer. The contact area must take into account the coating material accumulated around the contact. The model developed for elastic-plastic asperity contact by Chang [18] is illustrated in

Figure 8 (b). His model determines the contact area of the substrate as if no coating were present, and then adds in the extra area contributed by the deformed coating. The contact radius of the bare substrate can be found for elastic contact to be

$$a_s = (\delta_s R)^{1/2} \tag{10}$$

The contact radius of the substrate plus coating, a_c, is found from the Hertz solution by solving the implicit equation

$$t = \frac{1}{\pi R}\left[a_s\left(a_c^2 - a_s^2\right)^{\frac{1}{2}} - (2a_s^2 - a_c^2)\tan^{-1}\left(\frac{a_c^2}{a_s^2}-1\right)^{\frac{1}{2}} \right] \tag{11}$$

Once the contact radius is known, the contact area and force are computed as

$$A = \pi a_c^2 \tag{12}$$

$$P = \frac{4}{3}ER^{\frac{1}{2}}\delta^{\frac{1}{2}} + H_c\pi(a_c^2 - a_s^2) \tag{13}$$

In the equation for contact force, Eq (13), the first term represents the force supported by the substrate and the second term is the contribution from the coating. The effective microhardness of the coating must be used for H_c to account for the variation of hardness in the coating.

When the substrate deforms plastically, Eq (11) can be used again to find the contact radius, a_c; however, the bare substrate contact is modified for the plastic deformation in this case:

$$a_s = \left[\delta_s \left(2 - \frac{\delta_c}{\delta_s} \right) \right]^{\frac{1}{2}} \tag{14}$$

The indentation into the substrate is denoted by δ_s, which is δ_c−t. The contact area is also found in the same manner for plastic deformation as in Eq (12). However, the equation for contact load is

$$P = \pi R Y \delta_s \left(2 - \frac{\delta_c}{\delta_s} \right) \left[3 + \left(\frac{2}{3} K - 3 \right) \frac{\delta_c}{\delta_s} \right] + H_c \pi (a_c^2 - a_s^2) \tag{15}$$

The detailed derivation of these equations can be found in Chang [18]. The preceding equations (Eqs (5)-(15)) allow the computation of the contact area and pressure for a single asperity. In order to determine the total contact area and load for a surface, the areas and loads for each individual asperity must be summed.

The surface deformation model described above is combined with the constriction resistance model described in Merrill and Garimella [21] to enable the prediction of total contact resistance through a joint. This constriction resistance model analyzes heat flow through a coated semi-infinite cylinder terminating in the frustum of a cone, which approximates the geometry of a surface asperity. The results of this analysis are correlated in an equation using the geometry and thermal properties of the asperity as inputs.

To summarize the thermomechanical model used in this work, a surface deformation model first reduces the two rough surfaces to a flat surface and an equivalent rough surface, and then finds the total contact area by guessing a mean separation between the two contacting surfaces. The total contact area and load are computed for this mean separation, and the computed load is compared to the actual contact load. The separation distance is iterated upon until the computed load matches the actual load to within a certain tolerance. Once the deformed geometry is known, the constriction resistance is computed for each contacting asperity. The constriction resistance for each asperity is summed in parallel to find the total contact resistance.

Model Validation and Predictions

15

Predictions of contact resistance from the thermomechanical model developed in this work are presented and discussed here. The numerical results are compared to those obtained using the model in [7] as well as the current experiments. Table 5 lists the material properties used in the predictions (only some of which are needed for the model in [7]). The surface characteristics of the samples used in the experiments are listed in Table 6.

Predictions obtained from the two models above are shown in Figure 9 for a number of the substrate-coating pairs tested. These are a representative sample of all the comparisons, and serve to highlight general trends. Both models capture the general trend of decreasing contact resistance as the load is increased. Neither model has a consistently lower error with respect to the measurements for all cases, with one performing better in selected cases than the other.

The current model provides excellent predictions for hard coatings, such as nickel, whereas the Antonetti and Yovanovich model performs better for soft coatings. Likewise, as the roughness increases, the predictions from the current model are more accurate. In situations where a rough surface may be coated with a relatively hard coating, the current model is recommended. Although the current model tends to over-predict resistance at the lowest loads considered, the predictions are quite good for loads at the higher end of the range. **In the case of the silver coating on an aluminum substrate, neither model predicted the measured values very well. This lack of agreement may be attributed to the difficulty in ensuring a high-quality coating of silver on aluminum. The effect of coating quality on contact resistance is an area for potential future research.**

The current model provides insights into the mechanisms governing the contact resistance of a coated surface by predicting the number and size of contact spots, as well as computing the constriction resistance through individual spots. This yields improved predictions in cases where a statistical surface representation such as that used in [7] does not fully represent the actual surface. These situations include surfaces that have a relatively hard coating, or where the surfaces are very rough. With better surface metrology, improvements can be expected from the current model.

CONCLUSIONS AND RECOMMENDATIONS

A Design of Experiments (DOE) approach was used to investigate the effects of metallic coatings on thermal contact resistance. The experiment design considered five parameters:

16

substrate material, surface roughness, coating material, coating thickness and contact load. Fourteen samples were tested over a range of contact loads. A regression equation developed from the experimental results can be used for the prediction of contact resistance of coated joints. Some key conclusions from the experimental study include:

1. The coating thickness needed for the greatest contact resistance mitigation depends greatly on the substrate material, surface roughness, and coating material. A general optimum coating thickness cannot be prescribed.

2. The coating material and substrate material have a strong interaction. Thus, the effect on contact resistance of the coating material is dependent on the substrate material.

3. The quality of a coating may be the single most important factor with some coating materials. If the coating oxidizes or is very porous, large resistance to heat transfer can result.

The primary design parameters in most applications are the choice of coating material, coating thickness, and sometimes, substrate properties and metrology. The results of this study clearly show that the substrate hardness, thermal conductivity and roughness are very important parameters, irrespective of the presence of a coating.

A constriction resistance model was combined with a surface deformation analysis based on the deformation of a coated surface when indented with a spherical indenter. This model assumed purely plastic deformation in the coating, elastic deformation in the substrate if the deformation was less than the elastic limit, and elastic-plastic deformation past the elastic limit. The model used the surface generation method developed by Singhal et al. [5] to generate a three-dimensional surface from two-dimensional surface scans, and then computed the mean plane separation, actual contact area and contact radius of individual contacting asperities.

These models were combined into an integrated thermomechanical model to predict contact resistance across a pair of coated surfaces in contact. The main inputs to the code are surface scans of the surfaces in contact, material properties of the substrate and coating, coating thickness and nominal contact area. The output is contact resistance as a function of load. The key accomplishment of this code is the accurate prediction of contact resistance for contacts with rough surfaces or with relatively hard coatings. The code also gives fairly good predictions for other cases.

17

Acknowledgements

REFERENCES

1 Bowden, F.P. and Tabor, D., *The Friction and Lubrication of Solids*, Oxford University Press, London, 1950, pp. 20-32.

2 Singhal, V. and Garimella, S.V. "Prediction of Thermal Contact Conductance by Surface Deformation Analysis," in *Proceedings of International Mechanical Engineering Congress and Exposition*, New York, IMECE2001/HTD-24376, pp. 1-8, November 2001.

3 Yovanovich, M.M. and Antonetti, V.W., "Application of Thermal Contact Resistance Theory to Electronic Packages," *Advances in Thermal Modeling of Electronic Components*, Vol. 1, 1988, pp. 79-128.

4 Madhusudana, C.V., *Thermal Contact Conductance*, Springer-Verlag, New York, 1996.

5 Singhal, V., Litke, P. J., Black, A. F. and Garimella, S. V., "An Experimentally Validated Thermo-mechanical Model for the Prediction of Thermal Contact Conductance," *International Journal of Heat and Mass Transfer*, Vol. 48, 2005, pp. 5446-5459.

6 Parmenter, K.E and Marschall, E., "Influence of Surface Preparation on Thermal Contact Conductance of Stainless Steel and Aluminum," *Experimental Heat Transfer*, Vol. 8, 1995, pp. 185-208.

7 Antonetti, V.W. and Yovanovich, M.M., "Enhancement of thermal contact conductance by metallic coatings: Theory and experiment," *Journal of Heat Transfer*, Vol. 107, 1985, pp. 513-519.

8 Kang, T. K., Peterson, G. P., and Fletcher, L.S., "Effect of Metallic Coatings on the Thermal Contact Conductance of Turned Surfaces," *Journal of Heat Transfer*, Vol. 112, 1990, pp. 864-871.

9 Chung, K-C., "Experimental Study on the Effect of Metallic-Coated Junctions on Thermal Contact Conductance," *JSME International Journal*, Series B, Vol. 38, 1995, pp. 100-107.

10 Chung, K-C. and Sheffield, J.W., "Enhancement of Thermal Contact Conductance of Coated Junctions," *AIAA Journal of Thermophysics and Heat Transfer*, Vol. 9, 1995, pp. 329-334.

11 Li, Y.Z., Madhusudana, C.V. and Leonardi, E., "Enhancement of Thermal Contact Conductance: Effect of Metallic Coating," *AIAA Journal of Thermophysics and Heat Transfer*, Vol. 14, 2000, pp. 540-547.

12 Peterson, G.P. and Fletcher, L.S., "Measurement of the Thermal Contact Conductance and Thermal Conductivity of Anodized Aluminum Coatings," *Journal of Heat Transfer*, Vol. 112, 1990, pp. 579-585.

13 Lambert, M.A., Marotta, E.E. and Fletcher, L.S., "The Thermal Contact Conductance of Hard and Soft Coat Anodized Aluminum," *Journal of Heat Transfer*, Vol.117, 1995, pp. 270-275.

14 Cecco, V.S. and Yovanovich, M.M., "Electrical Measurement of Joint Resistance at Perfect Contact Interfaces: Application to Joint Conductance," *AIAA 10th Aerospace Sciences Meeting*, San Diego, CA., 1972.

15 *DOE KISS 97*, Copyright 1997 Digital Computations Inc. and Air Academy Associates, LLC.

16 Yovanovich, M.M., Hegazy, A.H. and DeVaal, L., "Surface Hardness Distribution Effects Upon Contact Gap and Joint Conductances," *AIAA-82-0887*, Joint AIAA/ASME Heat Transfer, Fluids and Thermophysics Conference, June 1982.

17 Automation Creations, Inc., *MatWeb-The Online Materials Information Resource*, 2005, http://www.matweb.com.

18 Chang, W.-R, "An Elastic-Plastic Contact Model for a Rough Surface with an Ion-Plated Soft Metallic Coating," *Wear*, Vol. 212, 1997, pp. 229-237.

19 Tian, H. and Saka, N., "Finite Element Analysis of an Elastic-Plastic Two-layer Half-Space: Normal Contact," *Wear*, Vol. 148, 1991, pp. 47-68.

20 Chang, W.-R., Etison, I. and Bogy, D.B., "An Elastic-Plastic Model for the Contact of Rough Surfaces," *Journal of Tribology*, Vol. 109, 1987, pp. 257-293.

21 Merrill, C.T. and Garimella, S.V., "Analysis and Prediction of Constriction Resistance between Coated Surfaces," *AIAA Journal of Thermophysics and Heat Transfer*, Vol. 20, 2006, pp. 346-348.

NOMENCLATURE

A   area (m^2)
DOE   design of experiments
E   Young's modulus (Pa)
H   hardness (VHN)
k   thermal conductivity (W/mK)
K   yield coefficient)
P   load (Pa)
Q   heat flow through a contact area (W)
R   resistance (K/W)
R   radius of curvature (m)
Ra   center-line average roughness (μm)
Rq   RMS roughness (μm)
T   temperature (K)
t   thickness (μm)
U   uncertainty
Y   yield strength (Pa)

Greek
δ   indentation depth (μm)
Δ   change in a value
ν   Poisson's ratio

Subscripts/Superscripts
0   nominal
1   pertaining to surface 1
2   pertaining to surface 2
c   coating, critical
coating   pertaining to the coating
contact   pertaining to the contact
g   gas
jump   temperature jump
s   substrate
′   effective

Table 1. Test matrix generated using a Design of Experiments approach. Roughness values are nominal, with the exact values given in Table 5.

Sample pair	Substrate	Roughness	Coating	Coating thickness
1	Al	1 µm	Ag	3 µm
2	Al	15 µm	Ag	5 µm
3	Al	5 µm	Ag	1 µm
4	Al	1 µm	Ni	1 µm
5	Al	15 µm	Ni	5 µm
6	Al	1 µm	Sn	5 µm
7	Al	15 µm	Sn	1 µm
8*	Br	1 µm	Ag	1 µm
9	Br	5 µm	Ni	3 µm
10	Cu	1 µm	Ag	3 µm
11	Cu	15 µm	Ag	1 µm
12	Cu	1 µm	Ni	5 µm
13	Cu	15 µm	Ni	1 µm
14	Cu	1 µm	Sn	1 µm
15	Cu	15 µm	Sn	5 µm

* This sample was discarded due to difficulties with the prepared sample

Table 2. Figure of Merit for coatings and substrates used in the experiments.

Substrates				Coatings			
	k (W/mK)	VHN (kgf/mm^2)	k/H		k (W/mK)	VHN (kgf/mm^2)	k/H
Cu	376	85	4.42	Ag	429	40	10.73
Al	184	120	1.53	Sn	67	10	6.70
Brass	98	149	0.66	Ni	90	367	0.25

Table 3. Microhardness values from tests on polished samples.

Coating	Measured microhardness (VHN)	Bulk hardness (VHN)	Substrate	Measured microhardness (VHN)	Bulk hardness (VHN)
Ni	390	75	Al	120	107
Ag	75	25	Cu	275	90
Sn	12	2.5	Brass	149	127

Table 4. Equations for hardness for several coating/substrate combinations. For t/d > 4.9, H′ = H$_c$.

<table>
<tr><td colspan="2">Ag on Cu</td><td colspan="2">Ag on Al</td></tr>
<tr>
<td>$\dfrac{t}{d} \leq 1$</td>
<td>$H' = H_s\left(1 - \dfrac{t}{d}\right) + 0.264 H_l \dfrac{t}{d}$</td>
<td>$\dfrac{t}{d} \leq 1$</td>
<td>$H' = H_s\left(1 - \dfrac{t}{d}\right) + 1.436 H_l \dfrac{t}{d}$</td>
</tr>
<tr>
<td>$1 < \dfrac{t}{d} \leq 4.9$</td>
<td>$H' = H_l\left(-0.219\dfrac{t}{d} + 1.36\right)$</td>
<td>$1 < \dfrac{t}{d} \leq 4.9$</td>
<td>$H' = H_l\left(-0.360\dfrac{t}{d} + 1.765\right)$</td>
</tr>
<tr><td colspan="2">Sn on Al</td><td colspan="2">Ni on Al</td></tr>
<tr>
<td>$\dfrac{t}{d} \leq 1$</td>
<td>$H' = H_s\left(1 - \dfrac{t}{d}\right) + 0.22 H_l \dfrac{t}{d}$</td>
<td>$\dfrac{t}{d} \leq 1$</td>
<td>$H' = H_s\left(1 - \dfrac{t}{d}\right) + 0.5 H_l \dfrac{t}{d}$</td>
</tr>
<tr>
<td>$1 < \dfrac{t}{d} \leq 4.9$</td>
<td>$H' = H_l\left(-0.156\dfrac{t}{d} + 1.545\right)$</td>
<td>$1 < \dfrac{t}{d} \leq 4.9$</td>
<td>$H' = H_l\left(0.22\dfrac{t}{d} + 0.26\right)$</td>
</tr>
</table>

Table 5. Material properties used for predictions from the model [17].

Material	Young's modulus (GPa)	Poisson's ratio	Hardness (VHN)	Yield strength (MPa)	Conductivity (W/mK)
Al	68.9	0.33	120	392	184
Brass	97	0.31	149	486.73	98
Cu	110	0.35	275	898.33	376
Ag	76	0.37	76	248.27	429
Ni	207	0.31	390	1274	90
Sn	41.4	0.33	12	39.2	67

Table 6. Metrology for the experimental samples.

Sample	1	2	3	4	5
Substrate	Al	Al	Al	Al	Al
Substrate Hardness (VHN)	120	120	120	120	120
Ra of sample A (µm)	0.87	11.23	5.66	1.11	12.91
Ra of sample B (µm)	0.82	11.31	4.35	1.10	12.86
Rq of sample A (µm)	1.02	14.13	5.43	1.37	16.08
Rq of sample B (µm)	1.09	14.04	7.07	1.39	16.14
Slope of sample A (rad)	0.24	0.30	0.26	0.23	0.36
Slope of sample B (rad)	0.30	0.32	0.24	0.23	0.36
Coating	Ag	Ag	Ag	Ni	Ni
Coating thickness (µm)	3	5	1	1	5
Coating Hardness (VHN)	76	76	76	390	390

Sample	6	7	8	9	10
Substrate	Al	Al	Brass	Brass	Cu
Substrate Hardness (VHN)	120	120	149	149	275
Ra of sample A (µm)	1.47	14.00	2.15	9.24	1.92
Ra of sample B (µm)	3.64	15.27	1.28	4.29	1.31
Rq of sample A (µm)	4.54	19.09	1.60	5.36	1.63
Rq of sample B (µm)	1.84	17.50	2.69	11.55	2.40
Slope of sample A (rad)	0.22	0.33	0.34	0.36	0.26
Slope of sample B (rad)	0.25	0.36	0.24	0.25	0.32
Coating	Sn	Sn	Ag	Ni	Ag
Coating thickness (µm)	5	1	1	3	3
Coating Hardness (VHN)	12	12	76	390	76

| Sample	11	12	13	14	15
Substrate	Cu	Cu	Cu	Cu	Cu
Substrate Hardness (VHN)	275	275	275	275	275
Ra of sample A (µm)	11.52	1.57	14.10	4.78	15.12
Ra of sample B (µm)	11.82	1.37	13.15	1.57	14.73
Rq of sample A (µm)	14.77	1.72	16.44	1.97	18.41
Rq of sample B (µm)	14.40	1.96	17.62	5.98	18.90
Slope of sample A (rad)	0.39	0.24	0.39	0.29	0.41
Slope of sample B (rad)	0.42	0.24	0.39	0.24	0.39
Coating	Ag	Ni	Ni	Sn	Sn
Coating thickness (µm)	1	5	1	1	5
Coating Hardness (VHN)	76	390	390	12	12
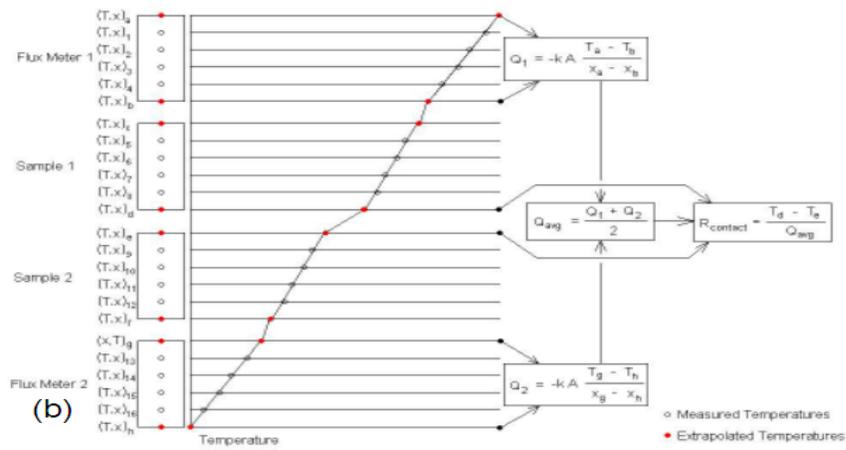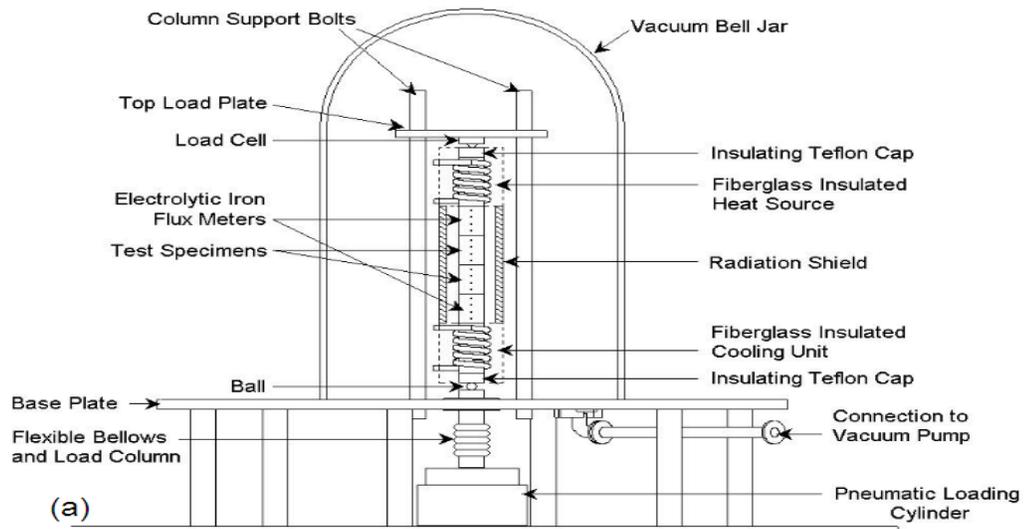
Figure 1. (a) Thermal contact conductance facility, and (b) graphical representation of the data analysis procedure.
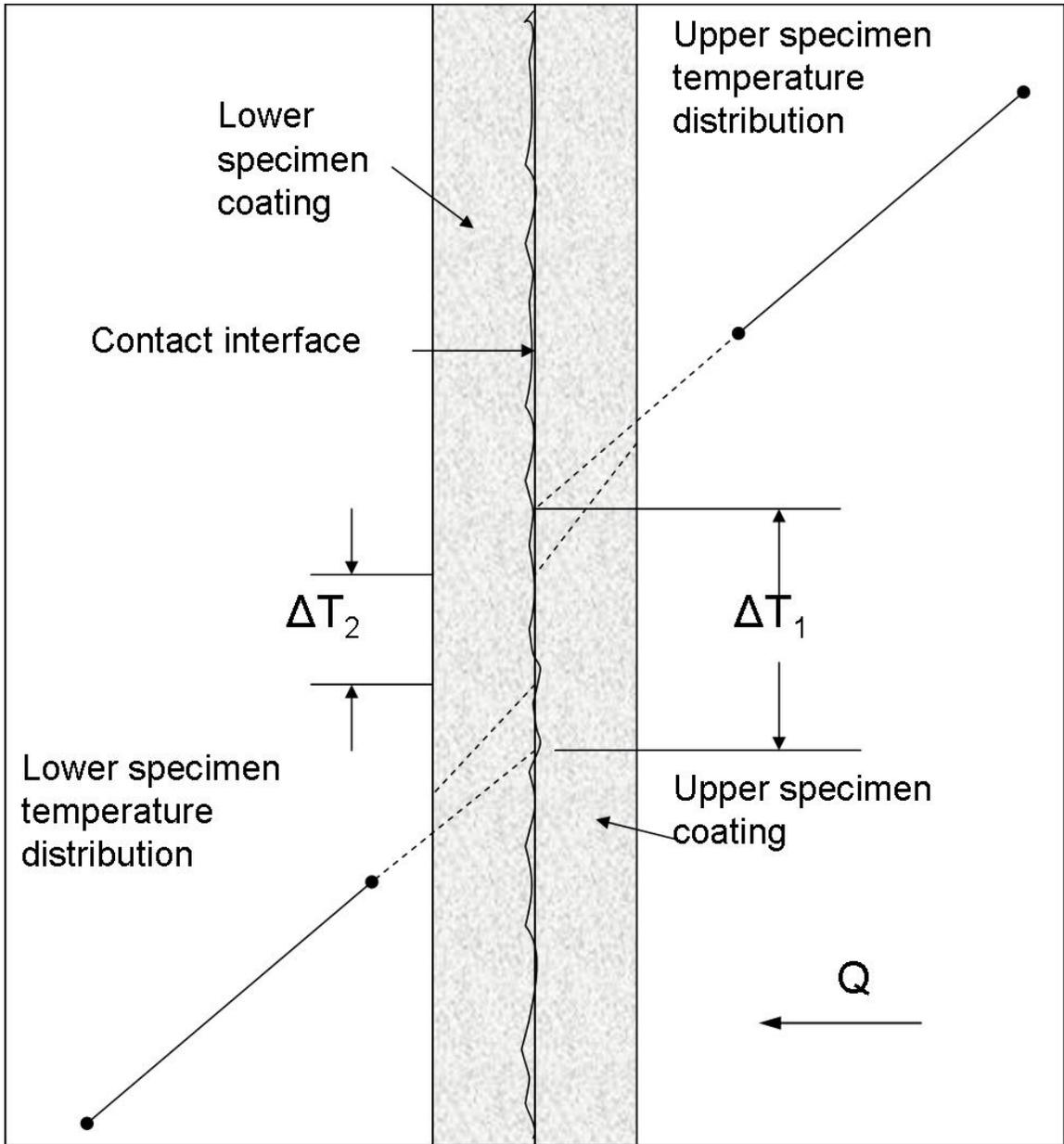
Figure 2. Extrapolation approaches to obtain interface temperatures; the differences indicated in the figure are greatly exaggerated for illustration.
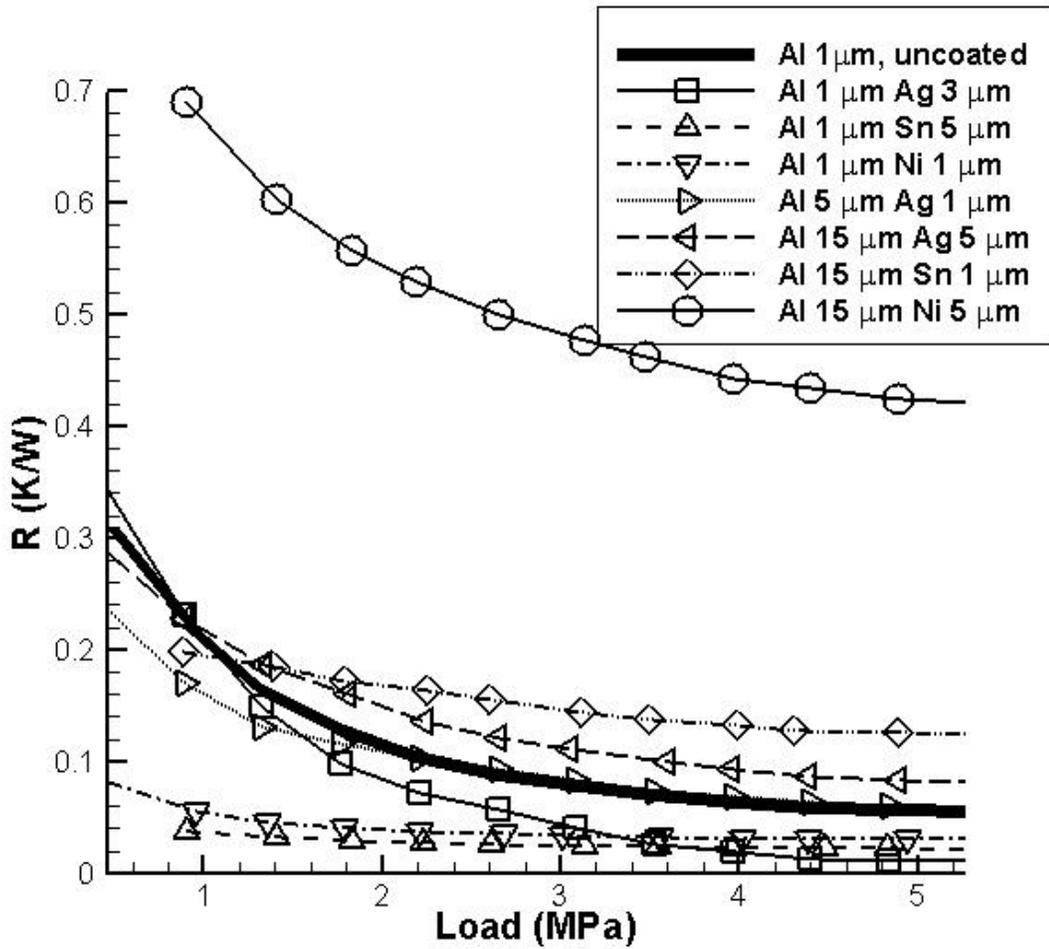
Figure 3. Contact resistance measurements on samples with aluminum substrates. Results are compared to a non-coated aluminum sample with a roughness of 1 μm Ra.
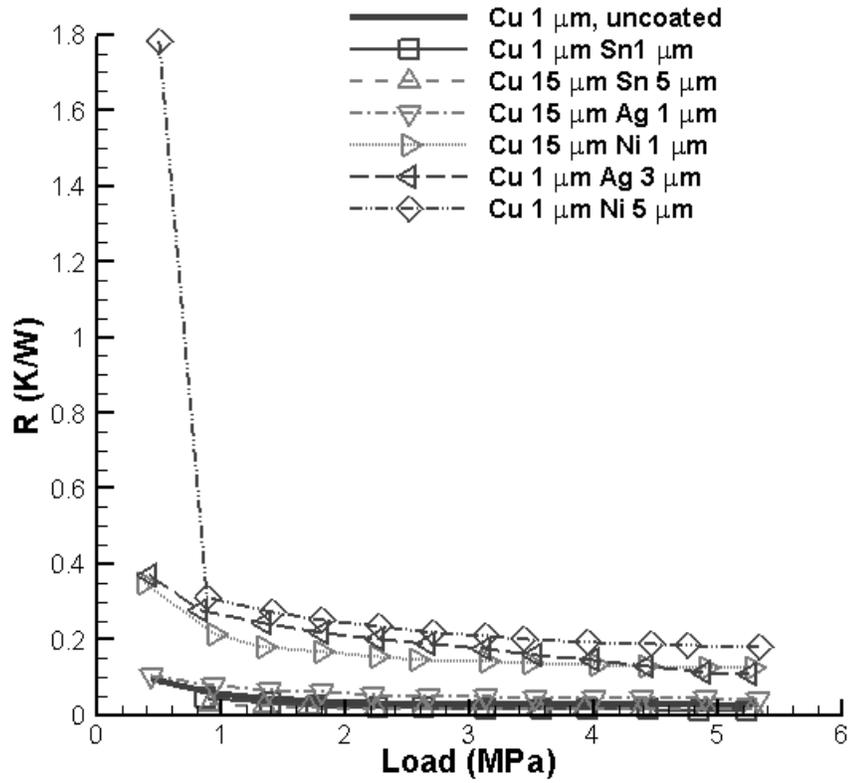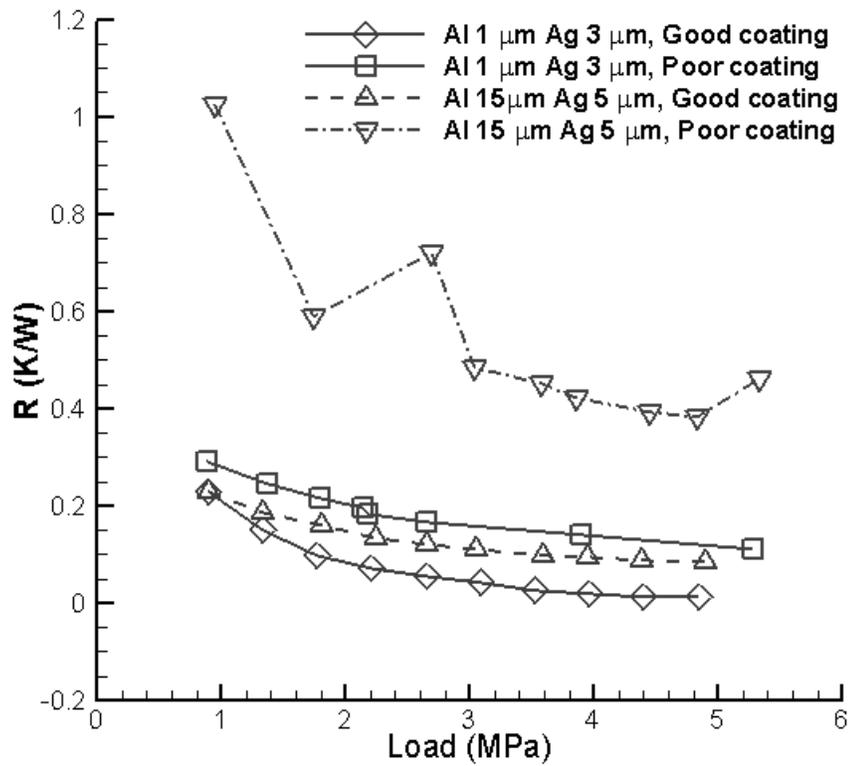
Figure 4. Contact resistance measurements on samples with copper substrates. Results are compared to a non-coated copper sample with a roughness of 1 μm Ra.

Figure 5. The effect of coating quality on contact resistance for two samples before and after re-coating.
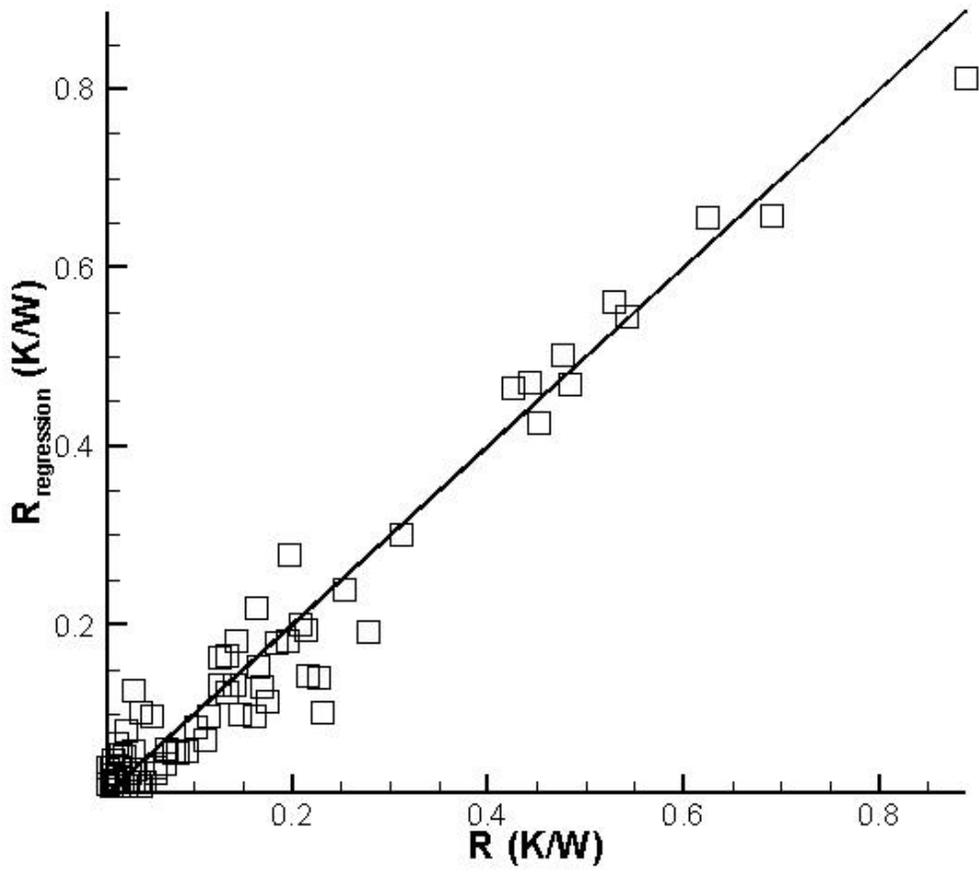
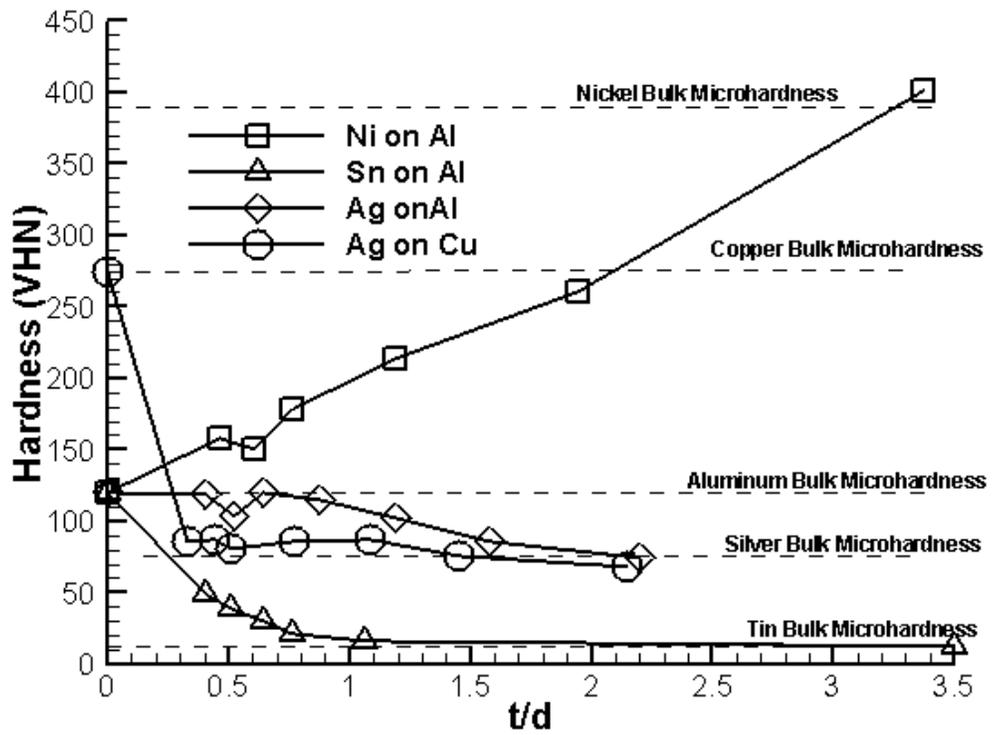Figure 6. Comparison of predictions from the DOE regression analysis with experimental results.

Figure 7. Hardness curves for silver coating on aluminum substrate, nickel coating on aluminum substrate, tin coating on aluminum substrate and silver coating on copper substrate.
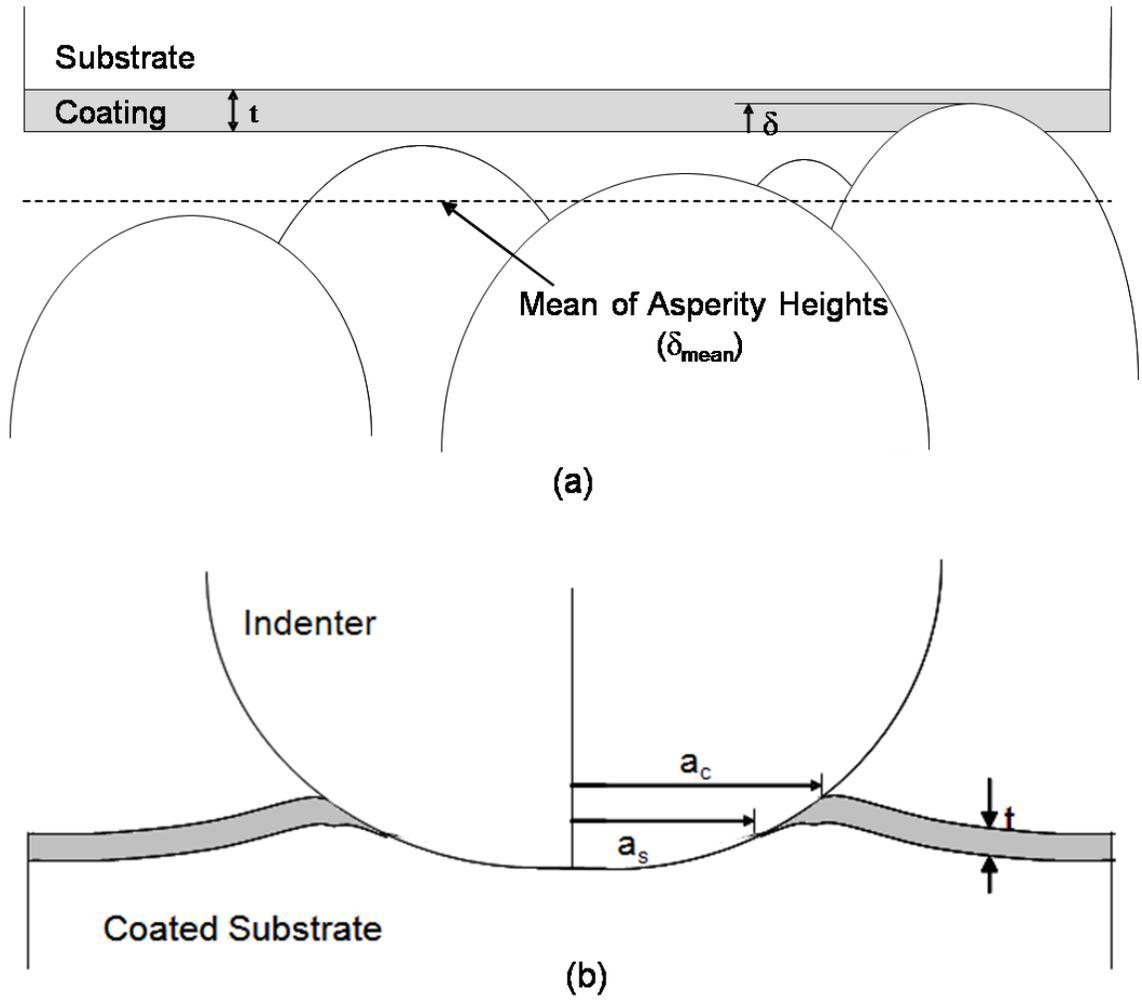
Figure 8. (a) A rough surface contacting a surface with a thin-film coating. (b) Deformed profile of an asperity contact. The asperity contact radius is determined by adding the radius of contact in the substrate and the extra radius supplied by the coating (adapted from Chang [18]).
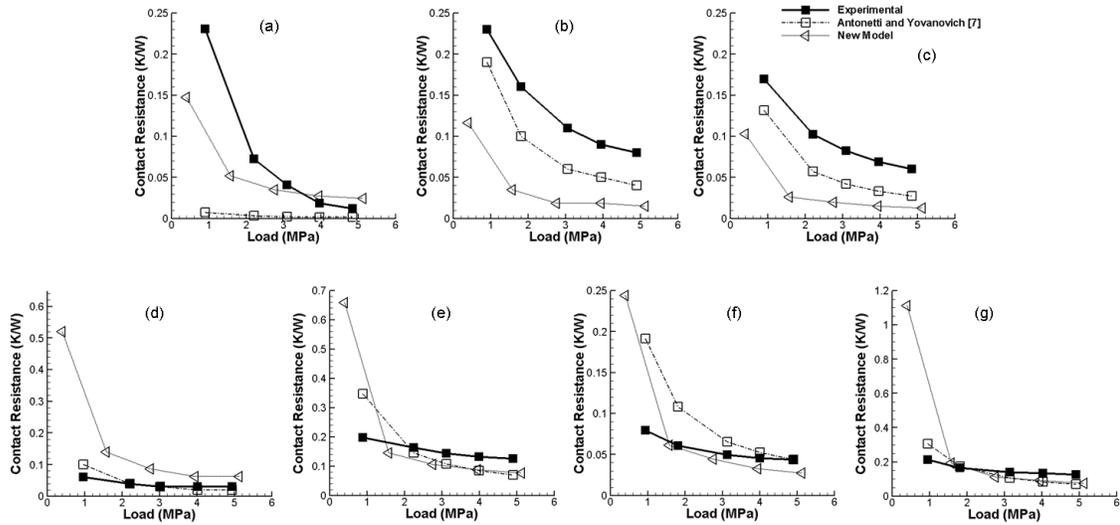
Figure 9. Comparison of predictions from the model developed in this work with the experimental results as well as the predictions from [7]: (a) 1 μm Ra Al with 3 μm Ag coating, (b) 15 μm Ra Al with 5 μm Ag coating, (c) 5 μm Ra Al with 1 μm Ag coating, (d) 1 μm Ra Al with 1 μm Ni coating, (e) 15 μm Ra Al with 1 μm Sn coating, (f) 15 μm Ra Cu with 1 μm Ag coating, and (g) 15 μm Ra Cu with 1 μm Ni coating.